Journal of Hazardous Materials 494 (2025) 138536

Contents lists available at ScienceDirect

Journal of Hazardous Materials

journal homepage: www.elsevier.com/locate/jhazmat

Region-specific characterization and ecotoxicity assessment of PAH compounds in winter $PM_{2.5}$ from three capital cities in Northeast Asia

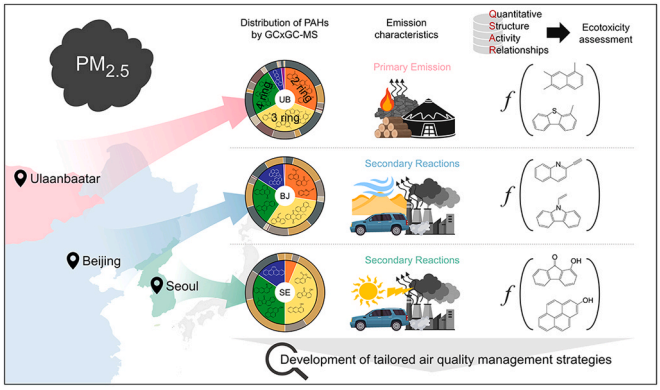
Min Sung Kim [a,b,1], Seulgidaun Lee [a,1], Moonhee Park [a,1], Hyemi Jang [a,c], Mira Choi [a,c], Ji Yi Lee [d], Mijung Song [e], Changhyuk Kim [f,g], Junyoung Ahn [h], Zhijun Wu [i], Amgalan Natsagdorj [j], Jungju Seo [k], Tae Kwon Lee [b], Young Hwan Kim [l,m,2,*], Kyoung-Soon Jang [a,c,n,3,**]

[a] Digital Omics Research Center, Korea Basic Science Institute, Cheongju 28119, Republic of Korea
[b] Department of Environmental Engineering, Yonsei University, Wonju 26493, Republic of Korea
[c] Division of Bio-Analytical Science, University of Science and Technology, Daejeon 34113, Republic of Korea
[d] Department of Environmental Science and Engineering, Ewha Womans University, Seoul 03760, Republic of Korea
[e] Department of Earth and Environmental Sciences, Jeonbuk National University, Jeonju 54896, Republic of Korea
[f] School of Civil and Environmental Engineering, Pusan National University, Pusan 46241, Republic of Korea
[g] Institute of Environment and Energy, Pusan National University, Pusan 46241, Republic of Korea
[h] National Institute of Environmental Research, Incheon 22689, Republic of Korea
[i] College of Environmental Sciences and Engineering, Peking University, Beijing 100871, China
[j] Department of Chemistry, National University of Mongolia, Ulaanbaatar 14201, Mongolia
[k] Division of R&D Equipment Industry, Korea Basic Science Institute, Daejeon 34133, Republic of Korea
[l] Research Center for Material Analysis, Korea Basic Science Institute, Daejeon 34133, Republic of Korea
[m] Graduate School of Analytical Science and Technology, Chungnam National University, Daejeon 34134, Republic of Korea
[n] Department of Plant Science and Technology, Chung-Ang University, Anseong 17546, Republic of Korea

HIGHLIGHTS

- Winter PAH profiles in $PM_{2.5}$ vary by region: Ulaanbaatar, Beijing, and Seoul.
- Ulaanbaatar has the highest PAHs, mainly from coal and biomass burning.
- Beijing and Seoul show more oxygenated/nitrogenated PAHs $_{via}$ secondary reactions.
- Seoul's hydroxylated PAHs show the highest ecotoxicity among three cities.

GRAPHICAL ABSTRACT



* Corresponding author at: Research Center for Material Analysis, Korea Basic Science Institute, Daejeon 34133, Republic of Korea
** Corresponding author at: Digital Omics Research Center, Korea Basic Science Institute, Cheongju 28119, Republic of Korea
E-mail addresses: yhkim@kbsi.re.kr (Y.H. Kim), ksjang@kbsi.re.kr (K.-S. Jang).
[1] These authors (Min Sung Kim, Seulgidaun Lee and Moonhee Park) equally contributed to this research.
[2] ORCID: 0000–0003-3478–8839
[3] ORCID: 0000–0001-5451–5788

https://doi.org/10.1016/j.jhazmat.2025.138536
Received 24 February 2025; Received in revised form 20 April 2025; Accepted 6 May 2025
Available online 7 May 2025
0304-3894/© 2025 The Author(s). Published by Elsevier B.V. This is an open access article under the CC BY license (http://creativecommons.org/licenses/by/4.0/).

ARTICLE INFO

Keywords:
Polycyclic aromatic hydrocarbons
Winter $PM_{2.5}$
Northeast Asia
Ecotoxicity assessment
Air quality management

ABSTRACT

Industrialization and urbanization in Northeast Asia have heightened $PM_{2.5}$ pollution, posing significant public health risks. This study examined the spatial and chemical variability of polycyclic aromatic hydrocarbons (PAHs) and their ecotoxicity in winter $PM_{2.5}$ from three capitals—Ulaanbaatar (UB, Mongolia), Beijing (BJ, China), and Seoul (SE, South Korea)—using two-dimensional gas chromatography time-of-flight mass spectrometry (GC×GC-TOF MS). $PM_{2.5}$ samples collected between December 15, 2020 and January 14, 2021 revealed UB had the highest concentrations (85.7 ± 36.7 μg m^{-3}) and PAH levels (758.9 ± 224.7 ng m^{-3}), primarily from coal combustion and biomass burning. BJ (30.3 ± 16.9 μg m^{-3}; 41.4 ± 18.4 ng m^{-3}) and SE (26.0 ± 14.4 μg m^{-3}; 6.2 ± 2.4 ng m^{-3}) had lower PAH levels but a higher share of secondary products, including oxygenated (OPAHs) and nitrogen-containing PAHs (NPAHs). Overall, 646 PAH compounds were identified: UB was dominated by methylated alkyl and sulfur-containing PAHs, while BJ and SE had more hydroxylated and carbonylated PAHs. QSAR ecotoxicity analysis indicated the highest toxicity in SE from hydroxylated PAHs and a broader toxic range in UB. These findings support air quality strategies to reduce coal combustion in UB and secondary PAH formation in BJ and SE.

1. Introduction

Air pollution remains a pressing environmental concern, particularly in densely populated regions like Northeast Asia [1]. The rapid industrialization and urbanization in these areas have led to elevated levels of particulate matter with a diameter of 2.5 micrometers or less ($PM_{2.5}$), primarily due to increasing anthropogenic activities, posing significant risks to human health and the environment [2–4]. $PM_{2.5}$ is of particular concern because of its ability to penetrate deeply into the respiratory system, resulting in numerous health complications, including respiratory and cardiovascular diseases, and even premature mortality [5,6]. The World Health Organization (WHO) has emphasized the urgency of reducing $PM_{2.5}$ levels to safeguard public health, particularly in regions suffering from high pollution [7].

Among the diverse components of $PM_{2.5}$, polycyclic aromatic hydrocarbons (PAHs) stand out due to their ubiquity, persistence, and detrimental health effects [8,9]. PAHs are a class of organic pollutants composed of multiple fused aromatic rings, often produced during incomplete combustion processes such as vehicle emissions, industrial activities, residential heating, and biomass burning. PAHs can be broadly categorized into parent (unsubstituted) PAHs and their derivatives, which include oxygenated PAHs (OPAHs), nitrated PAHs (NPAHs), alkylated PAHs, and sulfur-containing PAHs (SPAHs). Parent PAHs are typically formed through incomplete combustion of organic matter and are characterized by relatively lower reactivity but higher environmental persistence [10]. In contrast, PAH derivatives are often generated through atmospheric transformation processes such as photochemical oxidation and nitration, resulting in compounds with increased polarity, volatility, and in some cases, heightened toxicological activity. For example, OPAHs and NPAHs are more soluble in water and may exhibit enhanced oxidative stress potential compared to their parent compounds [11]. Alkylated and sulfur-containing PAHs, frequently observed in coal combustion emissions, can also demonstrate altered environmental behavior and bioavailability due to changes in molecular weight and functional group interactions [12,13]. This distinction is critical for understanding the atmospheric fate and ecotoxicological risks associated with complex PAH mixtures in urban environments.

PAHs are also categorized by their ring structures, with examples ranging from naphthalene (two rings) to benzo[*a*]pyrene (five rings), the latter being noted for its potent carcinogenicity [10]. Several PAHs are recognized as mutagenic, teratogenic, and carcinogenic, with some classified as probable or possible human carcinogens by the International Agency for Research on Cancer (IARC) [14]. In the health risk assessment of PAHs, cancer slope factor (CSF) and toxic equivalency factor (TEF) serve as critical tools for quantifying carcinogenic risk. The CSF enables estimation of cancer risk based on dose-response data [15], while TEF assigns relative potency values to PAHs in complex mixtures [16], with benzo[*a*]pyrene (BaP) widely used as the reference compound. However, these methods are limited by the lack of toxicity data for many PAH compounds, necessitating advanced approaches to refine risk assessment frameworks and better characterize the risks associated with comprehensive PAH exposure.

Recent advancements in toxicity assessment methodologies offer solutions to these challenges. Quantitative structure-activity relationship (QSAR) models predict the toxicity of chemical compounds based on molecular structure, serving as a valuable tool when experimental data are limited [17]. Interspecies correlation estimation (ICE) models complement QSAR by extrapolating toxicity data from surrogate species to other species, enhancing the robustness of predictions [18]. The integration of QSAR and ICE models has been shown to improve the derivation of predicted no-effect concentration (PNEC) values for ecological risk assessment [17]. Moreover, network toxicity models elucidate compound-gene-pathway interactions, providing a mechanistic understanding of PAH toxicity [19]. These advanced tools significantly enhance the precision of toxicity evaluations, addressing key gaps in the assessment of PAH-related risks [20,21].

The origins of PAHs in urban environments are diverse and complex. They can arise from both primary sources, such as direct emissions from vehicles and industrial activities, and secondary sources, formed through atmospheric reactions [22]. Additionally, PAHs are classified into petrogenic (from crude oil and petroleum products), pyrogenic (from high-temperature combustion), and biogenic (from natural processes such as wildfires) sources. By analyzing PAH concentrations and compositions, researchers can infer dominant pollution sources and assess the contributions of secondary formation processes [23–25]. This source-specific information is critical for developing effective mitigation strategies to reduce PAH levels and their associated risks in urban environments.

The concentration and composition of PAHs in $PM_{2.5}$ exhibit considerable seasonal and regional variability, particularly in winter. Heightened heating demands, increased cooking activities, and the operation of coal-fired power plants during winter exacerbate PAH emissions. This is especially pronounced in urban cities of Northeast Asia, where dense populations and extensive industrial activities intensify air pollution [23,26,27]. Despite the severity of winter air pollution in this region, previous studies have primarily focused on a limited subset of PAH compounds, leaving critical gaps in source apportionment and ecotoxicity assessment. Therefore, a comprehensive understanding of region-specific PAHs in winter $PM_{2.5}$ is essential to address these challenges.

This study aims to address these gaps by conducting a region-specific characterization and ecotoxicity assessment of PAH compounds in winter $PM_{2.5}$ samples from three capital cities in Northeast Asia: Ulaanbaatar (UB in Mongolia), Beijing (BJ in China), and Seoul (SE in South Korea). These cities were selected based on their strategic

locations along the East Asian westerlies, distinct energy infrastructures, and relevance to transboundary air pollution policymaking. While cities such as New Delhi also face severe air quality issues, the scope of this study was intentionally limited to Northeast Asia in alignment with the objectives of the Fine Particle Research Initiative in East Asia Considering National Differences (FRIEND), a multinational project led by South Korea to investigate the regional dynamics of $PM_{2.5}$. Importantly, the three study sites exhibit distinct fuel usage and heating infrastructures that influence their emission profiles. UB primarily relies on raw coal and biomass for residential heating, particularly in ger districts where centralized heating is unavailable, contributing to substantial primary emissions of PAHs and other combustion-related pollutants [28,29]. In contrast, BJ has implemented a widespread district heating system powered mainly by natural gas and cleaner fuels, supported by strong governmental mandates to phase out coal in urban cores [30,31]. SE utilizes mixed heating systems that include city gas, electric heating, and centralized networks, with comparatively stricter emission control regulations [32]. These differences in fuel types and heating practices provide a contextual basis for interpreting the regional variations in PAH concentrations and compositions observed in this study.

Unlike conventional studies that often rely on disjointed regional sampling efforts or limited targeted compound analyses, our study implemented a synchronized monitoring campaign across UB, BJ, and SE during the same winter period. At each site, real-time meteorological data, $PM_{2.5}$ concentrations, and gas-phase pollutants were continuously measured through on-line instruments, while filter-based $PM_{2.5}$ samples were simultaneously collected for detailed chemical characterization. All offline analyses, including organic and inorganic constituents in the particle phase, were performed by a centralized research team in South Korea using standardized protocols. Notably, comprehensive two-dimensional GC×GC-TOF MS profiling of 646 PAH compounds and QSAR-based ecotoxicity modeling were consistently applied across all samples. This integrated approach minimizes inter-laboratory variability and significantly enhances the reliability and comparability of chemical and toxicological data across regions. These methodological and organizational strengths establish a novel and robust framework for region-specific air pollution assessment in Northeast Asia.

2. Materials and methods

2.1. Monitoring sites and sampling $PM_{2.5}$

A simultaneous air quality monitoring campaign was conducted by the Fine Particle Research Initiative in East Asia Considering National Differences (FRIEND) project in three capital cities–Ulaanbaatar (UB) in Mongolia, Beijing (BJ) in China, and Seoul (SE) in Korea–across Northeast Asia from December 15, 2020, to January 14, 2021 (Fig. 1 A). The selection of UB, BJ, and SE was based on their status as the capital cities of Mongolia, China, and South Korea, respectively, where air pollution has become one of the most critical environmental concerns. Each city is regarded as a representative urban center experiencing severe $PM_{2.5}$-related issues within its national context, despite observable improvements in air quality in recent years attributable to the implementation of targeted pollution control policies [33,34]. Furthermore, the three cities are all geographically located along the prevailing westerlies, which dominate the regional atmospheric transport patterns in Northeast Asia. This alignment would support the investigation of not only localized emissions but also the influence of long-range transboundary pollution. To ensure environmental comparability, all sampling sites were located in central urban zones near residential areas and major roadways (within 30–500 m), and at similar elevations (e.g., rooftops or upper floors of university buildings), minimizing potential site-related biases.

$PM_{2.5}$ samples were collected daily over 23-hour periods using high-volume air samplers (models HV-1000R and HV-RW, SIBATA, Tokyo, Japan) at a flow rate of 1000 L min^{-1}, utilizing prebaked quartz microfiber filters (8 ×10 in., Pallflex Tissuequartz™, Pall Corporation, New York, USA). Sampling in UB was conducted on the rooftop of the main building of the National University of Mongolia (NUM), located at 47.55°N, 106.55°E, in the eastern sector of the city's central urban area [34]. The sampling site in BJ was established on the fourth floor of a building within the Changping campus of Peking University, China. This location is situated at coordinates 40.25°N, 116.19°E and approximately 500 m away from the major urban thoroughfares [22]. Sampling in SE was conducted at an intensive air quality monitoring site in the metropolitan area, located at coordinates 37.61°N, 126.93°E, approximately 30 m away from busy urban roads [35].

The $PM_{2.5}$ mass concentrations of the samples collected from the three regions were continually analyzed using a β-ray absorption technique [36]. After collection, the filters were stored in a −20°C freezer

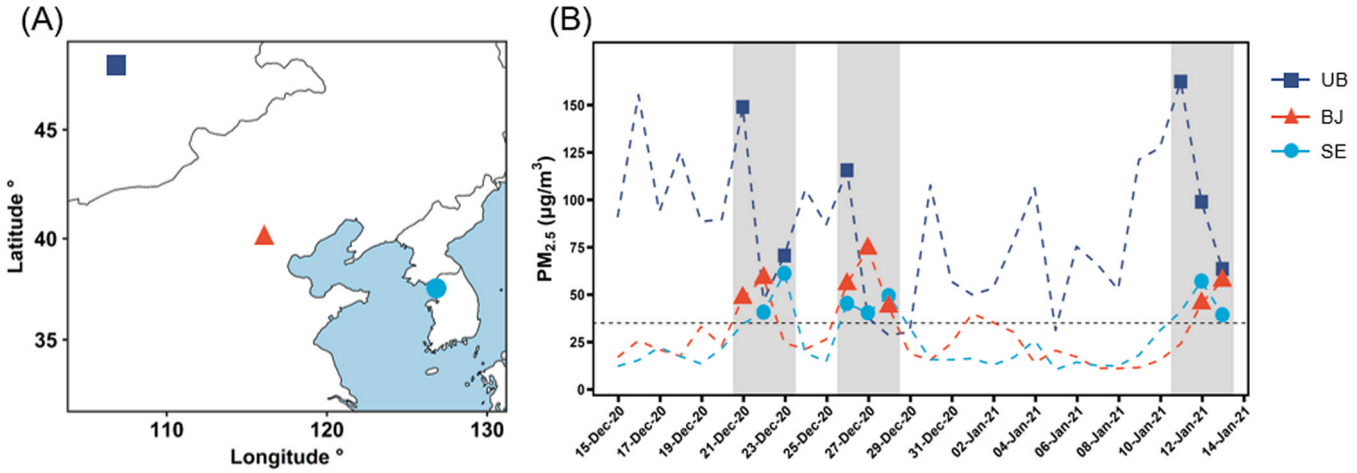


Fig. 1. (A) Geographical locations of the sampling sites and (B) daily averaged $PM_{2.5}$ concentrations during winter across three megacities in Northeast Asia. Observations were conducted from December 15, 2020, to January 14, 2021. Sampling sites include Ulaanbaatar (UB, navy square), Beijing (BJ, orange triangle), Seoul (SE, sky-blue circle). Haze episode days were identified based on days with elevated $PM_{2.5}$ concentrations across all three cities. In panel (B), dashed lines represent the daily $PM_{2.5}$ concentrations, and the overlaid symbols indicate the specific haze-episode days on which GC×GC-TOF MS analyses were performed for each city.

prior to analysis. A portion (10 cm^2) of the total filter area (516 cm^2) was used for the extraction of PAH compounds from the $PM_{2.5}$ samples. During the observation period, comprehensive meteorological conditions including temperature (Temp) and relative humidity (%RH) were recorded at each sampling site. Additionally, the concentrations of various air quality parameters were monitored, including $PM_{2.5}$, gaseous species [i.e., ozone (O_3), carbon monoxide (CO), nitric oxide (NO), and sulfur dioxide (SO_2)], particulate ions [i.e., ammonium (NH_4^+), nitrate (NO_3^-), and sulfate (SO_4^{2-})], and organic components [i.e., organic carbon (OC) and elemental carbon (EC)], as described previously [37]. The chemical attributes, including $PM_{2.5}$ mass concentration and environmental variables, are summarized in Supplementary Data Sheet 1.

Although the monitoring period overlapped with the COVID-19 pandemic, particularly during a time of reduced traffic and industrial activity, we took this into account by integrating multiple lines of evidence. The analysis of air mass back trajectories, meteorological data, and chemical composition—particularly elevated levels of coal and biomass burning markers in UB—suggests that the observed PAH profiles primarily reflect regional heating practices rather than short-term anthropogenic fluctuations. Moreover, this study was part of the FRIEND project, a multinational initiative led by South Korea to examine wintertime $PM_{2.5}$ in Northeast Asia under synchronized monitoring conditions. Importantly, most offline chemical analyses were centrally performed by a specialized Korean research team, ensuring consistent data quality across the three cities.

2.2. Air mass transport analysis

The air mass backward trajectories arriving at the sampling sites were calculated to estimate the air mass transport history using the Hybrid Single-Particle Lagrangian Integrated Trajectory (HYSPLIT) model of the National Oceanic and Atmospheric Administration (NOAA) and meteorological data from the Global Data Assimilation System (GDAS) of the National Centers for Environmental Information (NCEI) database [38]. The 72-hour backward air mass trajectories were computed in 3-hour intervals using the HYSPLIT model, with an endpoint height of 100 m above ground level at the receptor site, as described in previous studies [39,40]. In total, 704 air mass backward trajectories were obtained during the sampling periods (winter: 480; summer: 304). To categorize the major air masses affecting the receptor sites, air mass backward trajectory data were clustered using an angle-based distance matrix, taking into account the distance between each pair of trajectories [41,42]. All computation steps were performed in R using the openair packages [43,44].

2.3. GC×GC-TOF MS analysis and data processing

For the extraction of organic compounds (OCs), a portion of each quartz filter was immersed in a 3:1 (v/v) mixture of dichloromethane (DCM) and methanol (MeOH) and subjected to ultrasonic agitation. The resulting OC extracts were then filtered using a 0.45 μm PTFE syringe filter to remove insoluble materials, and the filtrates were dried under a gentle nitrogen stream. The dried samples were then dissolved in toluene for high-resolution two-dimensional gas chromatography time-of-flight mass spectrometric (GC×GC-TOF MS) analysis, as described previously [45].

The extracts were analyzed using a GC×GC-TOF MS system (LECO Pegasus 4D, Saint Joseph, MI) coupled with an Agilent 7890 A gas chromatograph equipped with a thermal modulator between the primary and secondary columns, with minor modifications to the previously described method [45–47]. Briefly, a 1 μL aliquot of the sample was injected in splitless mode, with the inlet temperature maintained at 250°C. Separation was performed using helium as the carrier gas at a constant flow rate of 1.2 mL min^{-1}, employing a Rxi-PAH column (30 m × 0.25 mm ID × 0.10 μm film; Restek, Bellefonte, PA) as the first column and a Rxi-17SilMS column (2 m × 0.25 mm ID × 0.25 μm film; Restek) as the second. The primary oven was programmed to hold at 60°C for 2 min, then ramped at 4°C min^{-1} to 300°C, and held for 10 min. A modulation period of 8 s was used, with the modulator temperature set at + 25°C relative to the secondary oven, and the secondary oven at + 15°C relative to the primary. The transfer line and electron impact (EI) ionization source were maintained at 250°C. Data acquisition was performed at a rate of 100 spectra per second, collecting within a mass range of m/z 35–520.

Data analysis was performed using LECO's ChromaTOF software (version 5.10), with compound identifications conducted by comparing EI mass spectral patterns with those in the Wiley and NIST libraries. Following the library search, compound identifications were based on the Similarity and Probability scores of the top 10 hits to determine the most probable compounds. The identification was further confirmed by using high-resolution data of molecular ion peaks within an accuracy of 5 ppm. Quantification was based on calibration curves constructed for 18 major PAHs within the range of 0.15–10 ppm, using the peak area ratio of each analyte to its internal standard.

To ensure analytical accuracy and precision, method validation and quality control procedures were implemented, as described previously [46]. Method detection limits (MDLs) and limits of quantification (LOQs) were determined for the 18 target PAHs based on signal-to-noise ratios of 3 and 10, respectively, and are presented in Table S1. Accuracy and precision were evaluated by spiking blank quartz filters (n = 3) with five deuterium-labeled PAH standards, including phenanthrene-d10, fluoranthene-d10, chrysene-d12, perylene-d12, and benzo[ghi] perylene-d12, and processing them identically to the field samples. The average recovery of these labeled standards was 100 %, ranging from 97 % to 105 %, with relative standard deviations (RSDs) between 1.5 % and 3.8 %. These results confirm the reliability of the extraction and quantification procedures. For non-targeted PAHs, qualitative identification was performed by EI mass spectral matching against NIST and Wiley libraries, and further validated using high-resolution molecular ion confirmation within ± 5 ppm mass accuracy.

2.4. Ecotoxicity assessment of identified PAHs

To assess the ecotoxicity of the identified PAH profiles, an integrated approach combining existing databases (i.e., US EPA ECOTOX database, https://cfpub.epa.gov/ecotox) and predictive modeling tools was utilized. When no data was available in the database, acute toxicity (lethal concentration 50, LC50) was predicted using OECD QSAR Toolbox (version 4.7.1) [48]. The methodology, based on Yordanova et al. [49], included input, profiling, data gathering, categorization, and gap filling. CAS numbers and SMILES codes of the identified PAHs were input into the QSAR Toolbox, and profiling was performed using its compound database. Aquatic toxicity endpoints, specifically LC50 values for mortality in *Pimephales promelas* (fathead minnow), were prioritized, and high-quality ecotoxicity data from the USEPA Duluth mortality database [50] were used for validation. For unknown components, structure-based predictions were iteratively refined using structural and mechanistic profilers to enhance consistency. Acute 96-hour toxicity predictions, focusing on LC50 values for *Pimephales promelas*, were generated to assess the potential ecological risks systematically. This comprehensive workflow integrates high-resolution profiling, database validation, and advanced predictive modeling, providing critical insights into the toxicity of known and unknown PAH compounds while informing targeted strategies for regional air quality management.

3. Results and discussion

3.1. Environmental characteristics of three capital cities in Northeast Asia during Winter of 2020

$PM_{2.5}$ concentrations varied significantly among the three cities, with UB recording the highest levels (85.7 ± 36.7 μg m^{-3}), followed by

BJ (30.3 ± 16.9 μg m^{-3}) and SE (26.0 ± 14.4 μg m^{-3}) (Fig. 1B). Daily $PM_{2.5}$ trends in BJ and SE showed overlapping haze episodes, which we attribute to shared regional-scale meteorological conditions. Although the timing of peak concentrations may differ slightly due to the geographic separation, both cities were frequently affected by similar air masses during haze episodes. Haze episodes, defined as days with daily mean $PM_{2.5}$ concentrations exceeding 35 μg m^{-3}, were identified during three key periods: December 21–23, December 26–28, 2020, and January 11–13, 2021.

As shown in Figure S1, UB's severe winter conditions, with average temperatures of −22.3°C, likely drove the intensive use of household heating, particularly in coal-burning stoves [51], contributing to elevated emissions of primary combustion pollutants such as carbon monoxide (CO, 1541 ppb), nitrogen monoxide (NO, 58.1 ppb), and sulfur dioxide (SO_2, 71.0 ppb). In contrast, BJ (453 ppb for CO and 1.1 ppb for SO_2) and SE (369 ppb for CO and 1.0 ppb for SO_2) recorded significantly lower levels of these pollutants, particularly carbon monoxide and sulfur dioxide, which are indicative of incomplete combustion and sulfur-rich fuel use, respectively. These differences reflect variations in fuel types and heating systems, with BJ and SE relying less on raw coal and more on cleaner and regulated energy sources. Meteorological factors also varied, with UB exhibiting the highest relative humidity (RH, 63.6 ± 3.5 %), which may have enhanced particle-phase reactions and influenced the chemical composition of $PM_{2.5}$ [52,53].

Particulate ion composition further highlighted regional differences. UB displayed the highest sulfate (SO_4^{2-}) levels (7.81 μg m^{-3}), linked to coal-fired power plants and household stove use [54–56], whereas BJ and SE showed higher nitrate (NO_3^-) levels, reflecting traffic emissions and secondary aerosol formation [57,58]. UB also exhibited the highest organic carbon (OC, 42.9 μg m^{-3}) and elemental carbon (EC, 1.5 μg m^{-3}) levels, suggesting dominant contributions from organic-rich combustion sources. In contrast, BJ and SE had higher fractions of inorganic salts, consistent with urbanized and industrialized emission profiles [59,60].

3.2. Air mass transport history analysis in three capital cities

Air mass transport patterns played a pivotal role in influencing haze episodes and pollutant characteristics across the three cities. The Hybrid Single-Particle Lagrangian Integrated Trajectory (HYSPLIT) model was used to estimate the air mass trajectories, allowing for accurate assessment of long-range pollutant transport. Although daily $PM_{2.5}$ trends in BJ and SE showed temporal offsets due to geographical distance, our HYSPLIT backward trajectory analysis (Fig. 2) suggests that both cities were frequently influenced by similar regional air masses during haze episodes, supporting the notion of common transboundary transport mechanisms under shared synoptic-scale meteorological conditions. However, it is important to note that HYSPLIT modeling may have limitations under complex meteorological conditions, such as rapidly changing wind patterns or localized atmospheric inversions.

UB was primarily affected by fast-moving northwest air masses originating from the Altai Mountains (C1 in Fig. 2A), which carried relatively clean air but, combined with the city's valley geography and frequent thermal inversions, trapped locally emitted pollutants near the surface [61–63]. This unique combination of transport patterns and geographical factors exacerbated $PM_{2.5}$ levels during haze episodes. BJ's air mass transport history was more complex, with a significant influence from fast-moving air masses originating in the Gobi Desert and northern China (C2 and C1 clusters in Fig. 2B). These air masses carried mineral dust, contributing to particulate pollution. Additionally, local emissions from industrial activities and traffic further amplified pollution levels during haze episodes. SE, on the other hand, experienced slow-moving westward air masses traversing the North China Plain and the Yellow Sea (C3 in Fig. 2C). This prolonged transport path likely facilitated the accumulation of secondary pollutants, contributing to elevated $PM_{2.5}$ levels during specific episodes. These findings underscore the importance of regional air mass dynamics in shaping pollution characteristics. The interplay between transport patterns and local emissions highlights the need for region-specific strategies to mitigate air pollution.

3.3. Comprehensive PAH profiles in three capital cities

The total PAH concentrations in $PM_{2.5}$ exhibited significant regional variability across the three capital cities, as shown in Fig. 3B. UB recorded the highest PAH burden (758.9 ± 224.7 ng m^{-3}), substantially

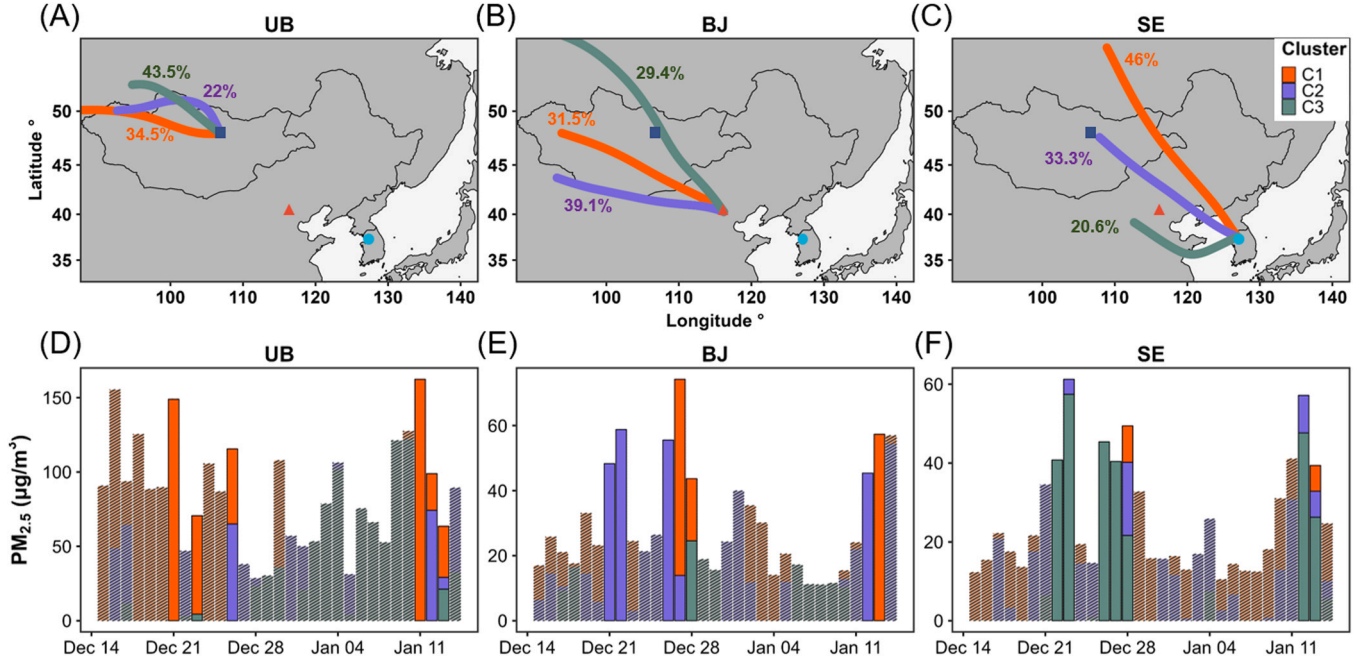


Fig. 2. Cluster analysis of air mass back-trajectories arriving at each sampling site during winter 2020. The top panel (A-C) visualizes the back-trajectories, while the bottom panel (D-F) presents daily average $PM_{2.5}$ concentrations, color-coded by the contribution rates of each cluster.

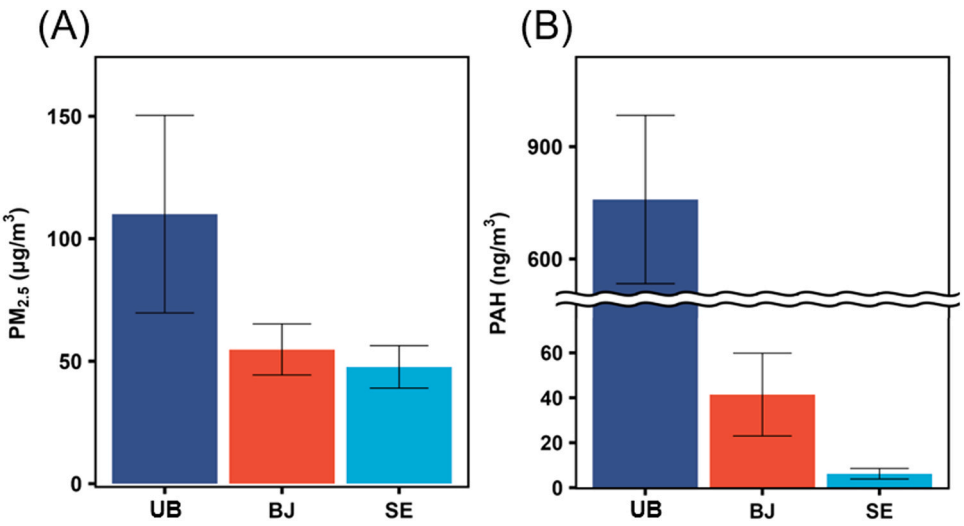


Fig. 3. Comparison of $PM_{2.5}$ mass concentrations and total PAH concentrations observed during haze episodes at the sampling sites.

exceeding concentrations observed in BJ (41.4 ± 18.4 ng m^{-3}) and SE (6.2 ± 2.4 ng m^{-3}). This pronounced disparity highlights the dominant influence of coal and biomass combustion in UB, where these fuels serve as primary energy sources for residential heating during winter [34]. This conclusion is further supported by the compositional characteristics of PAHs: UB exhibited a higher proportion of alkylated and sulfur-containing PAHs, which are indicative of direct emissions from raw coal and low-temperature combustion processes. In contrast, BJ and SE showed relatively lower total PAH concentrations but a greater share of OPAHs, such as anthraquinones and hydroxylated derivatives, suggesting enhanced atmospheric transformation processes under more oxidizing conditions. These differences in molecular composition align with each city's distinct energy use profiles and regulatory environments, and strengthen the interpretation of source contributions beyond mere concentration differences.

Comprehensive GC×GC-TOF MS analysis identified a total of 646 PAH compounds across the three cities. The corresponding chromatograms (Figure S2A-C) further corroborate these regional differences, revealing a substantially more diverse and intense PAH profile in UB compared to BJ and SE. Additionally, a Venn diagram (Figure S2D) illustrates the distribution of PAH species detected on event days, with 113 compounds common across all sites and 205, 138, and 32 region-specific PAH compounds uniquely identified in UB, BJ, and SE, respectively. Notably, region-specific PAH compounds accounted for 27.6 %, 18.8 %, and 18.6 % of the total PAH burden in UB, BJ, and SE, respectively, based on intensity-weighted data (Figure S3). Detailed information on the identified PAHs is summarized in Supplementary Data Sheets 2–5.

Figure S4 illustrates the compositional variations in PAH compounds detected across UB, BJ, and SE, categorized by ring structure (A) and PAH type (B). The comparison includes all detected PAHs (Total) and region-specific compounds (Region-specific). As shown in Figure S4A, when considering all PAHs identified in each of the three cities, there are no substantial differences in the overall distribution of PAH ring structures. However, a distinct divergence emerges in the composition of region-specific PAH compounds. Notably, in UB, 2-ring and 3-ring PAHs collectively constitute 66.8 % of the region-specific PAH burden (30.7 % and 36.1 %, respectively), whereas their proportions are significantly lower in BJ (27.5 % and 31.9 %, totaling 59.4 %) and SE (6.3 % and 43.8 %, totaling 50.1 %) (see Table S2). In contrast, high-molecular-weight PAHs (5- and 6-ring structures) account for a larger fraction in SE (15.6 % for 5-ring), compared to UB (6.8 %) and BJ (15.2 %), suggesting distinct emission sources and atmospheric transformation processes influencing the regional PAH profiles. Similarly, Figure S4B highlights more pronounced differences in PAH type distributions when considering region-specific compounds. While the overall PAH type composition remains relatively similar across the three cities for all detected compounds, region-specific PAHs exhibit distinct trends. The relative abundance of OPAHs is substantially higher in SE (62.5 %) compared to UB (12.7 %) and BJ (42.8 %), indicating a greater influence of secondary atmospheric oxidation processes. Conversely, UB exhibits the highest fraction of reduced PAHs (RPAHs) at 48.8 %, reinforcing the dominant contribution of direct combustion sources (see Table S3). These findings indicate that region-specific PAH signatures offer valuable insights into localized emission characteristics and transformation pathways. Therefore, these findings prompted a closer examination of region-specific PAH compounds to better understand the factors driving their compositional variability across the three cities.

3.4. *Region-specific characteristics of PAH compounds*

Fig. 4 further illustrates regional differences in PAH composition, focusing on the relationship between PAH types and their respective aromatic ring structures. In UB, the dominance of low-molecular-weight PAHs with two to three rings aligns with the widespread use of coal for household heating, which releases large amounts of incomplete combustion products. These PAHs, such as methylated naphthalenes and phenanthrenes, are indicative of coal-derived emissions. In contrast, BJ exhibited a higher fraction of four-ring PAHs, including pyrene and fluoranthene, which are commonly associated with vehicular exhaust and industrial combustion. SE, on the other hand, showed an even higher contribution of five- and six-ring PAHs, such as benzo[*a*]pyrene and indeno[1,2,3-cd]pyrene, reflecting the influence of gasoline and diesel combustion as dominant PAH sources.

Additionally, Fig. 4 reveals differences in PAH types across the three cities. UB had a significantly larger proportion of methylated PAHs, reinforcing the contribution of coal combustion, where alkylated PAHs are common byproducts. The sampling period overlapped with the COVID-19 pandemic, during which vehicular traffic and industrial activities were markedly reduced, especially in BJ and SE. Despite the overall decline in primary anthropogenic emissions, both cities exhibited a relative increase in oxygenated and nitrogen-containing PAHs (OPAHs and NPAHs), suggesting that atmospheric transformation processes remained active, and potentially intensified, due to altered photochemical oxidant levels and precursor availability. These findings indicate that even during periods of reduced human activity, the prevailing energy infrastructure and atmospheric reactivity play critical roles in shaping PAH transformation and toxicity profiles. While UB's

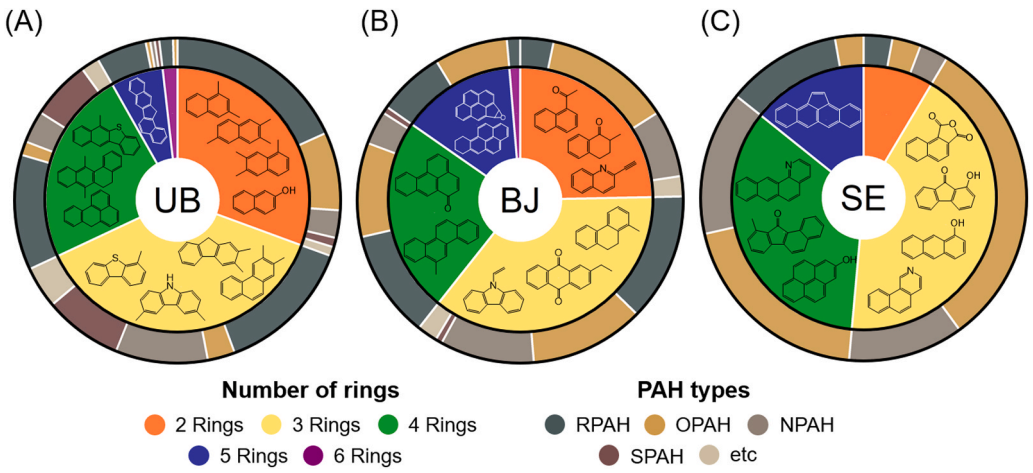


Fig. 4. Double donut charts depicting the relationship between PAH types and their respective aromatic ring structures, categorized by region (UB, BJ, and SE).

PAH composition remains strongly influenced by direct primary emissions, BJ and SE appear more susceptible to secondary transformation processes that chemically modify PAHs after emission.

The pandemic-induced reduction in emissions provided a unique opportunity to investigate how decreased primary emissions reshape the chemical composition of urban air pollution. The contrasting patterns—namely, the increase in transformation-derived PAHs in BJ and SE versus the continued dominance of coal combustion products in UB—highlight the influence of local infrastructure and atmospheric chemistry on pollutant profiles under atypical emission scenarios.

These findings underscore the importance of considering both total and region-specific PAH distributions when assessing urban air pollution. While general PAH profiles may appear similar across cities, the composition of region-specific PAHs provides critical insights into local emission sources and atmospheric transformation processes. UB's pollution is largely driven by coal combustion, requiring targeted controls on solid fuel use, while BJ and SE exhibit more complex emission profiles, necessitating mitigation strategies that address both primary emissions and secondary PAH formation.

To further interpret these region-specific patterns, source apportionment models could have provided quantitative insights. However, receptor models such as Positive Matrix Factorization (PMF) and Chemical Mass Balance (CMB), which are widely employed for such purposes, were not applicable in this study due to the nature of the dataset. The GC×GC-TOF MS analysis identified a large number of known and unknown PAH compounds, including alkylated, nitrogen-, and sulfur-containing derivatives, many of which lack standardized source profiles and emission factors essential for receptor modeling. Additionally, the identification confidence for several newly detected species does not meet the quantitative criteria required for reliable model input. Given these constraints, we focused on compositional patterns and diagnostic ratios to qualitatively infer potential emission sources. Future studies would benefit from the integration of receptor modeling techniques once more comprehensive and validated source profiles for emerging PAH compounds become available.

Overall, this study offers novel insights by capturing both the molecular-level diversity of PAHs across regions and the dynamic interplay between emission regimes and atmospheric processes under pandemic-modified environmental conditions. These findings provide a critical foundation for the development of adaptive air quality management strategies that remain effective in the face of evolving emission patterns and anthropogenic activity.

3.5. Structure-toxicity relationship and ecotoxicity distribution of PAH compounds

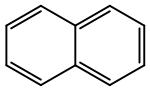
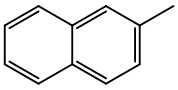
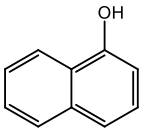
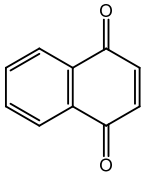
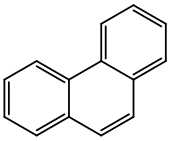
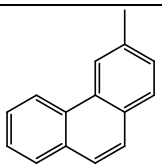
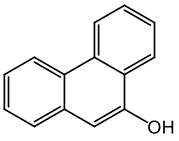
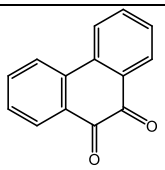
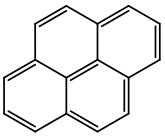
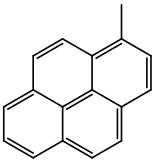
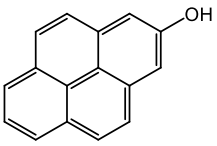
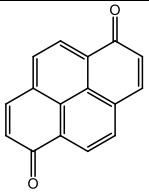
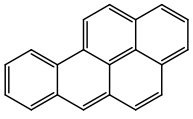
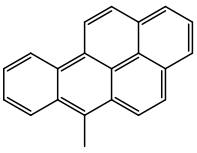
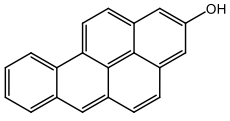
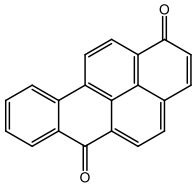
To comprehensively assess the ecotoxicity of PAH compounds, we employed QSAR modeling to predict LC50 values for compounds lacking experimental toxicity data. The structure-toxicity relationship was analyzed by considering the influence of aromatic ring size, functional group modifications, and regional emission characteristics across different urban regions. This approach enabled a broader toxicity assessment of both common and region-specific PAHs, including lesser-known derivatives not covered by traditional toxicological studies.

A clear trend emerged wherein an increase in aromatic ring size corresponded to enhanced toxicity. As summarized in Table 1, for example, naphthalene (2-rings, LC50: 20.0 μM) exhibited significantly lower toxicity than benzo[*a*]pyrene (5-rings, LC50: 0.0017 μM). This pattern aligns with prior findings that high-molecular-weight PAHs exhibit increased lipophilicity, facilitating bioaccumulation and cellular membrane permeability, and ultimately amplifying toxic effects in aquatic organisms [19]. Toxicity predictions were derived using the OECD QSAR Toolbox (version 4.7.1), a platform encompassing more than 944,000 aquatic toxicity data points across over 37,000 unique chemicals, including a wide array of PAH compounds. The toolbox enabled robust interpolation and read-across from structurally similar analogs, providing high-confidence LC_{50} estimates. Notably, well-characterized PAHs such as benzo[*a*]pyrene, fluoranthene, and phenanthrene are extensively represented in the Toolbox, further strengthening the validity of our modeled predictions. These QSAR-based estimates are thus grounded in an extensive empirical foundation and enhance the ecological relevance of our toxicity assessments.

Functional group modifications further modulated toxicity in a compound-specific manner. Methylation generally enhanced toxicity, as observed in 1-methylnaphthalene (LC50: 1.2 μM) compared to naphthalene (LC50: 20.0 μM), and 3-methylphenanthrene (LC50: 1.4 μM) compared to phenanthrene (LC50: 5.0 μM). In contrast, hydroxylation (-OH) and carbonylation (-C═O) demonstrated non-uniform effects, with some derivatives exhibiting reduced toxicity (e.g., 1,6-pyrenedione, LC50: 3.8 μM), while others maintained or slightly increased toxicity (e.g., 1-naphthol, LC50: 11.8 μM). These results suggest that while molecular size largely governs toxicity, functionalization can further modulate these effects in a compound-specific manner.

Beyond classical PAHs and their functionalized analogues, heteroatom-containing PAHs such as nitrogen-containing (NPAHs) and sulfur-containing PAHs (SPAHs), exhibited distinct toxicity patterns (see Table S4). Notably, benzo[*b*]naphtho[2,3-*d*]thiophene (LC50: 0.1387 μM) showed toxicity comparable to high-molecular-weight

Table 1
Structure-toxicity relationship of PAH scaffolds and functional group modifications.

Ring structure	Scaffold	Methylation	Hydroxylation	Carbonylation
2-Rings				
	Naphthalene (LC50: 20.0)	1-Methylnaphthalene (LC50: 1.2)	1-Naphthol (LC50: 11.8)	1,4-Naphthalenedione (LC50: 11.9)
3-Rings				
	Phenanthrene (LC50: 5.0)	3-Methylphenanthrene (LC50: 1.4)	Phenanthren-9-ol (LC50*: 2.7)	9,10-Phenanthrenedione (LC50: 11.0)
4-Rings				
	Pyrene (LC50: 0.046)	1-Methylpyrene (LC50*: 0.25)	Pyren-2-ol (LC50*: 1.27)	1,6-Pyrenedione (LC50*: 3.8)
5-Rings				
	Benzo[a]pyrene (LC50: 0.0017)	6-Methylbenzo(a)pyrene (LC50*: 0.016)	2-Hydroxybenzo(a)pyrene (LC50*: 0.28)	Benzo(a)pyrene-1,6-dione (LC50*: 0.58)

Values marked with an asterisk (*) are not experimentally determined but predicted using QSAR modeling in this study.

PAHs, underscoring the strong impact of sulfur substitution. The effect of methylation on SPAHs differed from that observed in other compound classes; for instance, both 6-methylbenzo[*b*]naphtho[2,3-*d*]thiophene (LC50: 0.83 μM) and 4-methyldibenzothiophene (LC50: 4.9 μM) exhibited reduced toxicity relative to their respective parent compounds. These observations emphasize the need to consider both molecular complexity and substitution patterns when evaluating PAH ecotoxicity.

To identify localized toxicity risks, we compared region-specific PAH compositions across three urban areas—UB, BJ, and SE—starting with UB, which exhibited the most toxic profile (Fig. 5). Region-specific PAHs in UB showed a substantial proportion of 2–3 ring alkylated derivatives with high toxicity (log LC50: −2 to −1). These species are likely linked to coal combustion, compounded by limited atmospheric degradation due to cold temperatures and high organic carbon concentrations that enhance PAH persistence on particulate matter. Notably, alkylation increased the toxicity of low-molecular-weight PAHs in UB, suggesting that assessments based solely on total PAH concentrations may underestimated health risks.

In contrast, BJ displayed an intermediate toxicity profile characterized by a narrower log LC50 range and a larger proportion of common PAHs. Region-specific compounds included several methylated 3-ring species, such as anthracene and phenanthrene derivatives, which showed moderate toxicity. The composition of PAHs in BJ reflects a mixture of sources, including coal combustion, industrial activities, and vehicular emissions, resulting in a complex but less extreme toxicity distribution. SE exhibited the highest LC50 values overall, indicating the lowest ecotoxicological risk among the three cities. However, the abundance of hydroxylated PAHs—particularly hydroxyl (-OH) derivatives of OPAHs, which accounted for ~50 % of OPAHs detected in

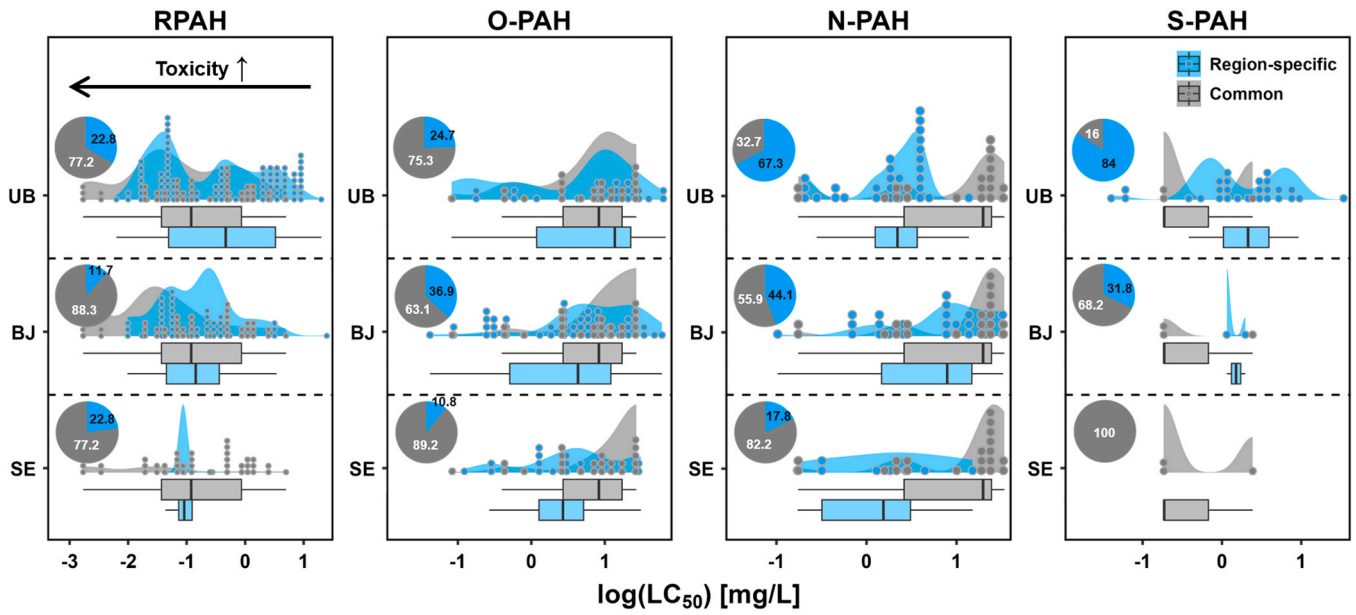


Fig. 5. Raincloud plots comparing the lethal concentration 50 (LC50) values for common and region-specific PAHs across three capital cities (UB, BJ, and SE) based on QSAR predictions. Each panel represents PAHs (total PAHs, OPAHs, NPAHs, and SPAHs), with the upper density plot illustrating LC50 distribution weighted by the concentrations of individual PAH components. The central boxplots display the median and interquartile range of LC50 values, while the lower scatter and histogram indicate individual data points and their frequency distribution. Pie charts indicate the proportion of region-specific (blue) and common (gray) PAHs in each category for the respective regions.

SE (Table S4)—raises concern. Hydroxylation has been associated with increased toxicity in certain lower-ring PAHs, as shown by QSAR predictions and prior studies [64,65]. This suggests that while SE's overall PAH mixture may appear less harmful, specific atmospheric transformation products could still pose significant localized risks.

Across all three cities, chemically modified 2–3 ring PAHs generally exhibited increased aquatic toxicity relative to their parent compounds, whereas structural modifications of 4–5 ring PAHs often led to reduced toxicity. This pattern corresponds to region-specific emission profiles and atmospheric transformation mechanisms. In UB, where low-ring PAHs from coal combustion dominate, functionalization processes (e.g., alkylation) tend to elevate toxicity. Meanwhile, in BJ and SE, higher emissions of 4–5 ring PAHs are more likely to undergo atmospheric aging and degradation, which often reduces toxicity via photolysis and phase partitioning.

Although human health risks from PAHs are strongly influenced by exposure concentrations and durations, this study focused on environmental toxicity due to limitations in available toxicological data. Among the 600 + PAH compounds detected, only a fraction has established carcinogenicity or inhalation toxicity profiles. In contrast, ecotoxicity data—particularly LC50 values—are more widely represented in databases and compatible with QSAR prediction tools. Therefore, we adopted an ecotoxicity-based framework to comparatively assess the environmental risks associated with region-specific PAH mixtures. While direct human health implications are beyond the scope of this work, the observed regional differences in toxicity profiles highlight the importance of localized monitoring and mitigation strategies, particularly for modified PAH derivatives that may exert elevated toxicological effects. Future research should aim to improve toxicity prediction models for functionalized PAHs and further evaluate their bioavailability and long-term ecological consequences.

4. Conclusions

This study provides a comprehensive characterization of PAH profiles in winter $PM_{2.5}$ across Ulaanbaatar (UB), Beijing (BJ), and Seoul (SE), revealing distinct regional differences in chemical composition, emission sources, and ecotoxicity. UB showed the highest PAH concentrations, primarily from coal and biomass combustion, with a dominance of methylated alkyl and sulfur-containing species. In contrast, BJ and SE had higher proportions of oxygenated and nitrogen-containing PAHs, reflecting enhanced secondary atmospheric transformation influenced by urban emissions.

Ecotoxicity assessments also varied by region. UB exhibited the broadest range of ecological risks due to diverse primary sources, while SE showed the highest compound-specific toxicity, mainly from hydroxylated PAHs linked to oxidative stress. These results underscore the need for region-specific air quality strategies: UB should transition from solid fuels to cleaner energy sources, while BJ and SE require stricter control of atmospheric precursors (e.g., NO_x, VOCs, ozone) to mitigate toxic secondary PAH formation.

Our approach, combining targeted analysis of 18 validated PAHs with untargeted screening of 600 + compounds, enabled a more comprehensive evaluation of both conventional and emerging PAHs. While the targeted compounds provided a reference for risk assessment, the inclusion of region-specific derivatives (e.g., OPAHs, NPAHs, SPAHs) revealed more nuanced patterns of toxicity and transformation. This highlights the importance of expanding compound validation, improving spectral libraries, and developing detailed source profiles for robust receptor modeling.

Despite its scope, the study also points to remaining challenges. Many emerging PAHs lack toxicological data, and interactions with other atmospheric pollutants are not fully understood. Addressing these gaps through experimental toxicology and international collaboration is critical for informing evidence-based air quality policies. Overall, our findings provide important insights into the chemical diversity and health risks of urban $PM_{2.5}$ and support the development of tailored strategies to reduce both the levels and toxicity of airborne PAHs in Northeast Asia.

Environmental implication

This study highlights significant regional disparities in polycyclic aromatic hydrocarbons (PAHs) within winter $PM_{2.5}$ across Northeast

Asia. Ulaanbaatar faces heightened ecological risks due to coal combustion-derived PAHs, necessitating urgent energy source transitions. Beijing and Seoul, while exhibiting lower PAH levels, show increased toxicity from secondary atmospheric transformations. Tailored mitigation strategies—such as curbing primary emissions in Ulaanbaatar and reducing secondary pollutant formation in Beijing and Seoul—are critical to protecting public health. These findings underscore the need for region-specific air quality management to address both the quantity and toxicity of PAHs in urban environments.

CRediT authorship contribution statement

Wu Zhijun: Validation, Formal analysis. **Ahn Junyoung:** Validation, Formal analysis. **Kim Min Sung:** Writing – original draft, Validation, Software, Formal analysis. **Seo Jungju:** Validation, Data curation. **Jang Kyoung-Soon:** Writing – review & editing, Supervision, Resources, Investigation, Funding acquisition, Formal analysis, Conceptualization. **Natsagdorj Amgalan:** Validation, Formal analysis. **Park Moonhee:** Methodology, Formal analysis. **Kim Young Hwan:** Writing – review & editing, Validation, Resources, Methodology, Formal analysis, Data curation. **Lee Seulgidaun:** Writing – original draft, Validation, Data curation. **Lee Tae Kwon:** Validation, Data curation. **Choi Mira:** Validation, Formal analysis, Data curation. **Jang Hyemi:** Validation, Software, Formal analysis. **Song Mijung:** Validation, Methodology, Data curation. **Lee Ji Yi:** Validation, Resources, Data curation. **Kim Changhyuk:** Validation, Methodology, Data curation.

Declaration of Competing Interest

The authors declare that the research was conducted in the absence of any commercial or financial relationships that could be construed as a potential conflict of interest.

Acknowledgements

This research was supported by the FRIEND (Fine Particle Research Initiative in East Asia Considering National Differences) Project through the National Research Foundation of Korea (NRF) funded by the Ministry of Science and ICT (2020M3G1A1114551) and KBSI (C512310 and C512110) grants.

Appendix A. Supporting information

Supplementary data associated with this article can be found in the online version at doi:10.1016/j.jhazmat.2025.138536.

Data availability

Data will be made available on request.

References

[1] Wang, Y., Tang, G., Zhao, W., et al., 2020. Different roles of nitrate and sulfate in air pollution episodes in the North China Plain. Atmos Environ 224, 117325. https://doi.org/10.1016/j.atmosenv.2020.117325.
[2] Chen, H., Deng, G., Liu, Y., 2022. Monitoring the influence of industrialization and urbanization on spatiotemporal variations of AQI and PM2.5 in three provinces, China. Atmosphere 13, 1377. https://doi.org/10.3390/atmos13091377.
[3] Jia, N., Li, Y., Chen, R., et al., 2023. A review of global PM2.5 exposure research trends from 1992 to 2022. Sustainability 15, 10509. https://doi.org/10.3390/su151310509.
[4] Yang, H., Yao, R., Sun, P., et al., 2023. Spatiotemporal evolution and driving forces of PM2.5 in urban agglomerations in China. Int J Environ Res Public Health 20. https://doi.org/10.3390/ijerph20032316.
[5] Mahiyuddin, W.R.W., Ismail, R., Sham, N.M., et al., 2023. Cardiovascular and respiratory health effects of fine particulate matters (PM2.5): a review on time series studies. Atmosphere 14, 856. https://doi.org/10.3390/atmos14050856.
[6] Garcia, A., Santa-Helena, E., De Falco, A., et al., 2023. Toxicological effects of fine particulate matter (PM2.5): health risks and associated systemic injuries-systematic review. Water Air Soil Pollut 234, 346. https://doi.org/10.1007/s11270-023-06278-9.
[7] World Health Organization (WHO), WHO global air quality guidelines: particulate matter (↱PM2.5 and PM10)↱, ozone, nitrogen dioxide, sulfur dioxide and carbon monoxide, in, 2021, pp. 290.
[8] Franchini, M., Mannucci, P.M., 2009. Particulate air pollution and cardiovascular risk: short-term and long-term effects. Semin Thromb Hemost 35, 665–670. https://doi.org/10.1055/s-0029-1242720.
[9] Sachdeva, K., Attri, A.K., 2008. Morphological characterization of carbonaceous aggregates in soot and free fall aerosol samples. Atmos Environ 42, 1025–1034. https://doi.org/10.1016/j.atmosenv.2007.10.002.
[10] Patel, A.B., Shaikh, S., Jain, K.R., et al., 2020. Polycyclic aromatic hydrocarbons: sources, toxicity, and remediation approaches. Front Microbiol 11, 562813. https://doi.org/10.3389/fmicb.2020.562813.
[11] Cao, W., Yuan, J., Geng, S., et al., 2023. Oxygenated and nitrated polycyclic aromatic hydrocarbons: sources, quantification, incidence, toxicity, and fate in soil—a review study. Processes 11, 52. https://doi.org/10.3390/pr11010052.
[12] Wnorowski, A., Harnish, D., Jiang, Y., et al., 2022. Assessment and characterization of alkylated PAHs in selected sites across Canada. Atmosphere 12, 1320. https://doi.org/10.3390/atmos13081320.
[13] Stout, S.A., Emsbo-Mattingly, S.D., 2008. Concentration and character of PAHs and other hydrocarbons in coals of varying rank – implications for environmental studies of soils and sediments containing particulate coal. Org Geochem 39, 801–819. https://doi.org/10.1016/j.orggeochem.2008.04.017.
[14] World Health Organization (WHO), List of Classifications Agents classified by the IARC Monographs, Volumes 1–134 in: i.a.f.r.o. cancer (Ed.) Monographs on the identification of carcinogenic hazards to humans, 2023.
[15] Knafla, A., Phillipps, K.A., Brecher, R.W., et al., 2006. Development of a dermal cancer slope factor for benzo[a]pyrene. Regul Toxicol Pharm 45, 159–168. https://doi.org/10.1016/j.yrtph.2006.02.008.
[16] Nisbet, I.C., LaGoy, P.K., 1992. Toxic equivalency factors (TEFs) for polycyclic aromatic hydrocarbons (PAHs). Regul Toxicol Pharm 16, 290–300. https://doi.org/10.1016/0273-2300(92)90009-x.
[17] Zheng, Z.Y., Ni, H.G., 2024. Predicted no-effect concentration for eight PAHs and their ecological risks in seven major river systems of China. Sci Total Environ 906, 167590. https://doi.org/10.1016/j.scitotenv.2023.167590.
[18] Wang, W., Jariyasopit, N., Schrlau, J., et al., 2011. Concentration and photochemistry of PAHs, NPAHs, and OPAHs and toxicity of PM2.5 during the Beijing Olympic Games. Environ Sci Technol 45, 6887–6895. https://doi.org/10.1021/es201443z.
[19] Wang, S., Li, C., Zhang, L., et al., 2024. Assessing the ecological impacts of polycyclic aromatic hydrocarbons petroleum pollutants using a network toxicity model. Environ Res 245, 117901. https://doi.org/10.1016/j.envres.2023.117901.
[20] Wu, B., Zhang, R., Cheng, S.P., et al., 2011. Risk assessment of polycyclic aromatic hydrocarbons in aquatic ecosystems. Ecotoxicology 20, 1124–1130. https://doi.org/10.1007/s10646-011-0653-x.
[21] Kumari, M., Kumar, A., 2022. Environmental and human health risk assessment of mixture of Covid-19 treating pharmaceutical drugs in environmental waters. Sci Total Environ 812, 152485. https://doi.org/10.1016/j.scitotenv.2021.152485.
[22] Kim, M.S., Wang, Y., Choi, M., et al., 2024. Comparison of secondary organic aerosol (SOA)-associated molecular features at urban sites in China and Korea in winter and summer (2019). Atmos Environ 318, 120235. https://doi.org/10.1016/j.atmosenv.2023.120235.
[23] Youn, N.R., Lee, S.J., Nguyen, T.N.T., et al., 2024. Seasonal variation, source identification, and health risk assessment of atmospheric polycyclic aromatic hydrocarbons (PAHs) in Ulsan, South Korea. Asian J Atmos Environ 18, 10. https://doi.org/10.1007/s44273-024-00032-1.
[24] Zhuo, S., Du, W., Shen, G., et al., 2017. Estimating relative contributions of primary and secondary sources of ambient nitrated and oxygenated polycyclic aromatic hydrocarbons. Atmos Environ 159, 126–134. https://doi.org/10.1016/j.atmosenv.2017.04.003.
[25] Balmer, J.E., Hung, H., Yu, Y., et al., 2019. Sources and environmental fate of pyrogenic polycyclic aromatic hydrocarbons (PAHs) in the Arctic. Emerg Contam 5, 128–142. https://doi.org/10.1016/j.emcon.2019.04.002.
[26] Sun, J., Shen, Z., Zhang, T., et al., 2022. A comprehensive evaluation of PM2.5-bound PAHs and their derivative in winter from six megacities in China: Insight the source-dependent health risk and secondary reactions. Environ Int 165, 107344. https://doi.org/10.1016/j.envint.2022.107344.
[27] Wu, D., Chen, L., Ma, Z., et al., 2024. Source analysis and health risk assessment of polycyclic aromatic hydrocarbon (PAHs) in total suspended particulate matter (TSP) from Bengbu, China. Sci Rep 14, 5080. https://doi.org/10.1038/s41598-024-55695-1.
[28] Batmunkh, T., Kim, Y.J., Jung, J.S., et al., 2013. Chemical characteristics of fine particulate matters measured during severe winter haze events in Ulaanbaatar, Mongolia. J Air Waste Manag Assoc 63, 659–670. https://doi.org/10.1080/10962247.2013.776997.
[29] Guttikunda, S., 2007. Urban Air Pollution Analysis for Ulaanbaatar. Elsevier, Washington, DC, USA.
[30] Lee, M., Chang, J., Deng, Q., et al., 2024. Effects of a coal to clean heating policy on acute myocardial infarction in Beijing: a difference-in-differences analysis. Lancet Planet Health 8, e924–e932. https://doi.org/10.1016/S2542-5196(24)00243-2.
[31] Lu, X., Zhang, S., Xing, J., et al., 2020. Progress of air pollution control in china and its challenges and opportunities in the ecological civilization era. Engineering 6, 1423–1431. https://doi.org/10.1016/j.eng.2020.03.014.

[32] Shim, C., Hong, J., 2016. Impact of a national plan for future electricity supply on ambient air quality in South Korea. Energy Policy 88, 278–288. https://doi.org/10.1016/j.enpol.2015.10.033.
[33] Jang, K.S., Choi, M., Park, M., et al., 2020. Assessment of PM2.5-bound nitrogen-containing organic compounds (NOCs) during winter at urban sites in China and Korea. Environ Pollut 265, 114870. https://doi.org/10.1016/j.envpol.2020.114870.
[34] Park, J.I., Kim, M.S., Yeo, M., et al., 2023. Chemical and morphological characterization by SEM–EDS of PM2.5 collected during winter in Ulaanbaatar, Mongolia. Atmos Environ 303, 119752. https://doi.org/10.1016/j.atmosenv.2023.119752.
[35] Kim, N.K., Kim, Y.P., Ghim, Y.S., et al., 2022. Spatial distribution of PM2.5 chemical components during winter at five sites in Northeast Asia: High temporal resolution measurement study. Atmos Environ 290, 119359. https://doi.org/10.1016/j.atmosenv.2022.119359.
[36] Choi, K., Yang, W., 2021. Psychological changes and cancer occurrence in Seoul citizens due to changes in fine dust concentration before seoul fine dust policy. Int J Environ Res Public Health 18. https://doi.org/10.3390/ijerph182111210.
[37] Ha, Y., Kim, J., S., L, et al., 2023. Spatiotemporal differences on the real-time physicochemical characteristics of PM2.5 particles in four Northeast Asian countries during Winter and Summer 2020–2021. Atmos Res 283, 106581. https://doi.org/10.1016/j.atmosres.2022.106581.
[38] Draxler, R.R., Hess, G.D., 1998. An overview of the HYSPLIT_4 modelling system for trajectories, dispersion, and deposition. Aust Meteor Mag 47, 295–308.
[39] Park, M., Wang, Y., Chong, J., et al., 2020. Simultaneous Measurements of Chemical Compositions of Fine Particles during Winter Haze Period in Urban Sites in China and Korea. Atmosphere 11, 292. https://doi.org/10.3390/atmos11030292.
[40] Choi, J.H., Jang, E., Yoon, Y.J., et al., 2019. Influence of biogenic organics on the chemical composition of Arctic aerosols. Glob Biogeochem Cycle 33, 1238–1250. https://doi.org/10.1029/2019GB006226.
[41] Bogawski, P., Borycka, K., Grewling, L., et al., 2019. Detecting distant sources of airborne pollen for Poland: Integrating back-trajectory and dispersion modelling with a satellite-based phenology. Sci Total Environ 689, 109–125. https://doi.org/10.1016/j.scitotenv.2019.06.348.
[42] Sirois, A., Bottenheim, J.W., 1995. Use of backward trajectories to interpret the 5-year record of PAN and O3 ambient air concentrations at Kejimkujik National Park, Nova Scotia. J Geophys Res -Atmos 100, 2867–2881. https://doi.org/10.1029/94JD02951.
[43] Carslaw, D.C., Ropkins, K., 2012. openair — An R package for air quality data analysis. Environ Model Softw 27-28, 52–61. https://doi.org/10.1016/j.envsoft.2011.09.008.
[44] R Core Team, R: A Language and Environment for Statistical Computing. R Foundation for Statistical Computing, Vienna, Austria, 2020, http://www.R-project.org/.
[45] Choi, J.H., Ryu, J., Jeon, S., et al., 2017. In-depth compositional analysis of water-soluble and -insoluble organic substances in fine (PM2.5) airborne particles using ultra-high-resolution 15T FT-ICR MS and GCxGC-TOFMS. Environ Pollut 225, 329–337. https://doi.org/10.1016/j.envpol.2017.02.058.
[46] Son, S., Park, M., Jang, K.S., et al., 2023. Comparative analysis of organic chemical compositions in airborne particulate matter from Ulaanbaatar, Beijing, and Seoul using UPLC-FT-ICR-MS and artificial neural network. Sci Total Environ 901, 165917. https://doi.org/10.1016/j.scitotenv.2023.165917.
[47] Cho, E., Park, M., Hur, M., et al., 2019. Molecular-level investigation of soils contaminated by oil spilled during the Gulf War. J Hazard Mater 373, 271–277. https://doi.org/10.1016/j.jhazmat.2019.03.084.
[48] Dimitrov, S.D., Diderich, R., Sobanski, T., et al., 2016. QSAR Toolbox - workflow and major functionalities. SAR QSAR Environ Res 27, 203–219. https://doi.org/10.1080/1062936X.2015.1136680.
[49] Yordanova, D., Schultz, T.W., Kuseva, C., et al., 2019. Automated and standardized workflows in the OECD QSAR Toolbox. Comput Toxicol 10, 89–104. https://doi.org/10.1016/j.comtox.2019.01.006.
[50] Risk Assessment of Chemicals, 2007. An Introduction, in. In: van Leeuwen, C.J., Vermeire, T.G. (Eds.), Risk Assessment of Chemicals: An Introduction. Springer, Dordrecht, Netherlands.
[51] Sumiya, E., Dorligjav, S., Purevtseren, M., et al., 2023. Climate patterns affecting cold season air pollution of Ulaanbaatar City, Mongolia. Climate 11, 4. https://doi.org/10.3390/cli11010004.
[52] Song, M., Jeong, R., Kim, D., et al., 2022. Comparison of Phase States of PM2.5 over Megacities, Seoul and Beijing, and Their Implications on Particle Size Distribution. Environ Sci Technol 56, 17581–17590. https://doi.org/10.1021/acs.est.2c06377.
[53] Seong, C., Kim, D., Jeong, R., et al., 2024. Influence of relative humidity and composition on PM2.5 phases in Northeast Asia. ACS Earth Space Chem 8, 788–797. https://doi.org/10.1021/acsearthspacechem.4c00019.
[54] Davy, P.K., Gunchin, G., Markwitz, A., et al., 2011. Air particulate matter pollution in Ulaanbaatar, Mongolia: determination of composition, source contributions and source locations. Atmos Pollut Res 2, 126–137. https://doi.org/10.5094/APR.2011.017.
[55] Guttikunda, S.K., Lodoysamba, S., Bulgansaikhan, B., et al., 2013. Particulate pollution in Ulaanbaatar, Mongolia. Air Qual Atmos Health 6, 589–601. https://doi.org/10.1007/s11869-013-0198-7.
[56] Hasenkopf, C.A., Veghte, D.P., Schill, G.P., et al., 2016. Ice nucleation, shape, and composition of aerosol particles in one of the most polluted cities in the world: Ulaanbaatar, Mongolia. Atmos Environ 139, 222–229. https://doi.org/10.1016/j.atmosenv.2016.05.037.
[57] Qin, Y.M., Tan, H.B., Li, Y.J., et al., 2017. Impacts of traffic emissions on atmospheric particulate nitrate and organics at a downwind site on the periphery of Guangzhou, China. Atmos Chem Phys 17, 10245–10258. https://doi.org/10.5194/acp-17-10245-2017.
[58] Qiu, Y., Wu, Z., Man, R., et al., 2023. Secondary aerosol formation drives atmospheric particulate matter pollution over megacities (Beijing and Seoul) in East Asia. Atmos Environ 301, 119702. https://doi.org/10.1016/j.atmosenv.2023.119702.
[59] Hong, X., Yang, K., Liang, H., et al., 2022. Characteristics of Water-Soluble Inorganic Ions in PM(2.5) in Typical Urban Areas of Beijing, China. ACS Omega 7, 35575–35585. https://doi.org/10.1021/acsomega.2c02919.
[60] Zheng, L., Wu, D., Chen, X., et al., 2024. Chemical profiles of particulate matter emitted from anthropogenic sources in selected regions of China. Sci Data 11, 1206. https://doi.org/10.1038/s41597-024-04058-6.
[61] Kim, M., Ha, Y., Kim, J., et al., 2024. First real-time size distribution measurements of aerosol particles in Mongolia. Atmos Environ 345, 121052. https://doi.org/10.1016/j.atmosenv.2025.121052.
[62] Batmunkh, T., Kim, Y.J., Jung, J.S., et al., 2013. Chemical characteristics of fine particulate matters measured during severe winter haze events in Ulaanbaatar, Mongolia. J Air Waste Manag Assoc 63, 659–670. https://doi.org/10.1080/10962247.2013.776997.
[63] Sanduijav, C., Ferreira, S., Filipski, M., et al., 2021. Air pollution and happiness: Evidence from the coldest capital in the world. Ecol Econ 187, 107085. https://doi.org/10.1016/j.ecolecon.2021.107085.
[64] Krzyszczak, A., Czech, B., 2021. Occurrence and toxicity of polycyclic aromatic hydrocarbons derivatives in environmental matrices. Sci Total Environ 788, 147738. https://doi.org/10.1016/j.scitotenv.2021.147738.
[65] Fallahtafti, S., Rantanen, T., Brown, R.S., et al., 2012. Toxicity of hydroxylated alkyl-phenanthrenes to the early life stages of Japanese medaka (Oryzias latipes). Aquat Toxicol 106-107, 56–64. https://doi.org/10.1016/j.aquatox.2011.10.007.